Cu-Mg-O thin films by RF magnetron co-sputtering: Their band offsets with CdS in heterojunction solar cells

K. C. Sanal[a,b*], Soorya Pushpan[c], P. K. Nair[a], and M. T. S. Nair[a]

[a]*Instituto de Energías Renovables, Universidad Nacional Autónoma de México,*

Priv. Xochicalco (S/N), Temixco, Morelos-62580, México.

[b]*Facultad de Ciencias Químicas, Universidad Autónoma de Nuevo León, Cd. Universitaria, San Nicolás de los Garza, Nuevo León , C.P. 66455, México.*

[c]*Facultad de Ingeniería Mecánica y Eléctrica, Universidad de Autónoma de Nuevo León, Av. Universidad, Cd. Universitaria, San Nicolás de los Garza, Nuevo León, México, 66455*

Recibido 30 septiembre2022, Aceptado 19 octrubre 2022

Resumen

We report on Cu-Mg-O thin films of 100 - 300 nm in thickness produced by radio frequency (RF) reactive sputtering from Cu and Mg-metal targets in an argon-oxygen ambient. The amount of Mg in the thin films was varied through changing the RF power applied at the Mg target. When the Mg content in the Cu-Mg-O film changed from 0 to 0.3, the optical bandgap increased from 1.73 eV to 2.13 eV, and the electrical conductivity decreased from 9 x 10^{-3} Ω^{-1} cm^{-1} (Cu_xO) to 6.7 x 10^{-5} Ω^{-1} cm^{-1} ($Cu_{0.7}Mg_{0.3}O$). Solar cells of these films, FTO/ CdS/$Cu_{0.85}Mg_{0.15}O$/C-Ag, showed a short circuit current density of 2.86 mA/cm^2, an open circuit voltage of 378 mV, and power conversion efficiency of 0.25%. X-ray photo-electron spectroscopy depth profile analyses of the interfaces suggest a negative conduction band offset in CdS/$Cu_{0.85}Mg_{0.15}O$ (– 0.74 eV) as well as in CdS/Cu_xO (– 0.9 eV) solar cells.

Palabras clave: Cu-Mg-O, thin film, rf sputtering, solar cell, XPS depth profile, band offset.

1. Introducción

Copper oxide is a well-known p-type semiconductor, known even before the era of Ge and Si. In the last few decades, it has been intensively investigated for its optoelectronic applications. There exist reports on CuO with reference to their electrical,[1] photo-electrochemical,[2] and photoluminescence[3] properties, as well as on their applications in solar cell,[4] gas sensor,[5] superconducting, [6] and as an antimicrobial [7] material. As a low-cost and non-toxic material with ease of producing thin films, CuO attracts industrial interest as well. The different methods to produce thin films of CuO are: RF sputtering, thermal evaporation, spin-coating, pulsed laser deposition, chemical vapor deposition, successive ionic layer adsorption and reaction (SILAR) and molecular beam epitaxy. [8–14]

The crystal structure of CuO is monoclinic, and it exhibits a direct energy bandgap (1.5 eV - 2 eV) with a large optical absorption coefficient in the visible region. The optical bandgap (E_g) in thin films of CuO can be tuned by incorporating other elements, as reported previously. [15,16] According to the first-principle calculations done by Nolan et al, [17] the substitutional doping of copper oxide with relatively larger cations such as Mg^{2+}, Sn^{2+}, Sr^{2+} or Ca^{2+} would lead to an increase in its optical band gap. Joao-Resende et al [18] reported Mg-doped Cu_2O as p-type transparent conductive oxide thin films. Mg-doped $CuCrO_2$ p-type films were also reported with a low electrical resistivity of 4.5 x 10^{-3} Ω cm.[19] Thin films of CuO show stronger optical absorption than that of Cu_2O in the visible region of the solar spectrum. However, relatively little is known on CuO heterojunction solar cells. Thin film of CuO sputtered on a semiconductor substrate is being used for typical heterojunction solar cells. Masudy-Panah et al, [20] in 2015, reported a heterojunction thin film solar cell with sputtered p-CuO in Al/Ti/n-Si/p-CuO/Ti/Al, with power conversion efficiency (PCE) of 1 % and subsequently showed[21] that by substituting the p-CuO layer with a Ti doped (0.009%) p-CuO in the cell resulted in an efficiency of 1.2 %. Apart from this, there is no report yet on thin film solar cells with doped CuO. Mixed phase of copper oxide nano powders can be used to improve the performance of heterojunction solar cells. Baumik et al[22] reported a solar cell structure, glass/ITO/ZnO/CuO/NP(Cu_2O, CuO), with a PCE of 2.88 %. Kaphle et al[23] reported in 2020 nanostructured ZnO(10% cobalt doped)/CuO

heterojunction solar cells with MoO_3 buffer layer with a PCE of 2.11 %.

The persistent interest in CuO as a solar cell absorber material is a perceived familiarity with the material, its low-cost and low-toxicity, and large-scale material availability to enter into production worldwide, when a viable solar cell structure is developed. With many different methods already available to produce the Cu_xO material, a versatile and accessible solar cell technology could emerge. In the search for a viable CuO solar cell technology, it is significant to understand the carrier transport mechanism at the interface of each layer of a solar cell structure. The defect density at the interface and the energy band offsets influence the photo-generated carrier recombination at interface. The prime novelty of the present work is the development of Cu-Mg-O thin films employing RF magnetron reactive co-sputtering technique for photovoltaic applications, with a CdS thin film as an n-widow layer. A benefit of introducing Mg in the CuO film in the solar cell structure by the RF sputter-deposition is seen in the relatively better performance of the FTO/CdS/$Cu_{0.85}Mg_{0.15}O$/C (PCE, 0.25 %) solar cell with respect to FTO/CdS/Cu_xO/C (PCE, 0.006%), arising from a nearly thirty-fold increase in the short circuit current density (J_{sc}) in the former (from 0.076 to 2.16 mA/cm^2) with an open circuit voltage (V_{oc}) of 378 mV. We are unable to ascertain whether the reactive sputter-deposition from the Mg and Cu targets modified the CdS surface through the formation of a CdS:Mg/Cu layer, which brings-in this advantage. We note that in a previous work,[23] a ZnO:Co/CuO interface was found as advantageous (PCE, 2.1%). We report the current-voltage characteristics as well as the band offsets at the Cu_xO/CdS and $Cu_{0.85}Mg_{0.15}O$/CdS interfaces, obtained from the X-ray photoelectron spectroscopy depth profile analysis. We hope the methodology and the results reported here would promote further work.

2. Experimental

We deposited Cu-Mg-O thin films on clean glass substrates using RF magnetron reactive co-sputtering from two 3" (7.62 cm) diameter targets of Cu (Kurt J. Lesker) and Mg (Kurt J. Lesker). Prior to starting the deposition, the sputter-chamber was evacuated to 5 x 10^{-5} torr base pressure. During the deposition, argon and oxygen gases (each of 99% purity from INFRA-gas) were introduced to the chamber at flow rates of 10 sccm and 2 sccm, respectively. During the sputter-deposition, the chamber pressure was maintained at 3.5 mtorr. A constant RF power (100 W) was applied on the Cu target, while that on the Mg target was changed from 0 to 250 W for the deposition of the thin films of varying compositions and thickness. The substrate holder kept at 10 cm from the sputtering targets rotated at 20 rpm during the deposition lasting for 60 min. The resulting thin films were specular and of uniform thickness, indicated by the uniform color tone in reflected daylight, of 100 - 300 nm in the different sputtering experiments. When the RF power was 240 or 250 W at the Mg-target, the film thickness dropped to smaller values.

We used a Rigaku D-Max 2200 diffractometer with Cu-K_α radiation to record the Grazing incidence X-ray diffraction (GIXRD) patterns of the films. A stylus profiler Dektak 6M unit was used in measuring the thin film thickness. A Shimadzu UV-VIS-NIR 3101 PC spectrophotometer was used to record the optical transmittance (T) and specular reflectance (R). For analyzing the chemical composition of the films by energy dispersive x-ray spectroscopy (EDS), we used a Bruker Quantax 200 EDX spectrometer attached to a FESEM, JEOL EOS 6701 equipment. The cross-sectional images of the solar cell structures were analysed using field emission scanning electron microscopy (FESEM) with Hitachi SU-8020 microscope. The surface morphology of the films was recorded by contact mode atomic force microscopy (AFM) on a Veeco Scanasyst series equipment. A computer interfaced electrical measurement unit consisting of a Keithley 619-Multimeter and a Keithley 230-Programmable voltage source recorded the electrical properties of the films. Ohmic contact on the film was made through conductive colloidal silver paint, dried at 75 °C in a laboratory oven for 30 min. For the photocurrent measurement, the samples were illuminated with a tungsten halogen lamp providing an intensity of 1000 W m^{-2} at the film surface. After stabilizing the current in the dark, the data were recorded by applying a bias of 5 V across a pair of coplanar silver paint electrodes for the first 20 s in the dark, the next 40 s under illumination, and finally the last 20 s after shutting the illumination off to record the dark-decay of the photocurrent. These data were converted to electrical conductivity (σ) using the sample thickness and the electrode geometry.

Solar cell development – Fluorine-doped tin oxide (FTO, TEC-8 Dyesol-Australia) substrate with a sheet resistance of 8 Ω was used to deposit the solar cells in superstrate configuration. Thin films of CdS with 320 nm in thickness were deposited on these substrates by three consecutive chemical bath depositions of 60-minute duration each, at 80 °C from a solution containing cadmium-citrate complex and thiourea, as described previously.[24] These films are of hexagonal crystalline structure with an E_g of 2.6 eV and a high photo-to-dark electrical conductivity ratio of 10^6. Subsequently, a thin film of p-$Cu_{0.85}Mg_{0.15}O$ of 360 nm thickness was deposited on the FTO/CdS. We also prepared solar cells using a 340 nm Cu_xO film as an absorbing layer, with a CdS film of 300 nm in thickness. Colloidal graphite paint in an acrylic base (SPI-Chem) was applied on the film as electrodes of 0.5 cm x 0.5 cm, area (0.25 cm^2), and colloidal silver paint on it for completing the solar cell. Figure 1 shows the cross-sectional view of the solar cell structures (a) FTO/CdS(320 nm)/$Cu_{0.85}Mg_{0.15}O$ (360 nm)/C-Ag and (b) FTO/CdS (300 nm)/Cu_xO (340 nm)/C-Ag, in which the demarcations of each layers of the solar cells with corresponding thickness are noted. Current-voltage characteristics of these solar cells were measured under simulated AM 1.5 G one-sun illumination (100 mW cm^{-2}) from a solar simulator (Oriel Sol 3A class AAA).

X-ray photoelectron spectra (XPS) depth profile analyses of the solar cells were done using a Thermo Scientific Surface analysis spectrometer. In order to record the XPS spectra from the interfaces of the solar cells into its depth, argon-ion etching (2 keV) with 1 nm/s etch rate was employed.

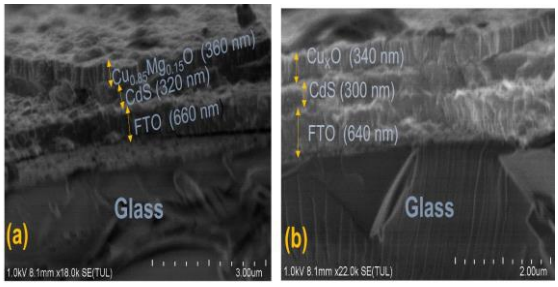

Figure 1: Cross-sectional FESEM images of solar cell structures (a) FTO/CdS(320 nm)/$Cu_{0.85}Mg_{0.15}O$ (360 nm)/C-Ag and (b) FTO/CdS (300 nm)/Cu_xO (340 nm)/C-Ag.

3. Results and discussions

3.1 Chemical composition and crystalline structure

Figure 2 shows the EDX spectra of the thin films of Cu_xO and Cu-Mg-O. The Mg content in Cu-Mg-O films increases as the RF power applied at the Mg-target increases from 0 – 250 W. The atomic compositions of Cu and Mg in the films were obtained from the emission spectra by the EDS software. We express the elemental composition in the films produced by applying a fixed RF power of 100 W at the Cu-target and different RF power at the Mg-target as: a) 0 W, Cu_xO; b) 100 W, $Cu_{0.93}Mg_{0.07}O$; c) 150 W, $Cu_{0.85}Mg_{0.15}O$; d) 200 W, $Cu_{0.84}Mg_{0.16}O$; and e) 250 W, $Cu_{0.70}Mg_{0.30}O$. Solar cells were produced under conditions a) and c). We describe below from the GIXRD results that the materials (b) – (e) are formed by the substitution of Cu-sites by Mg in CuO with a monoclinic crystalline structure.

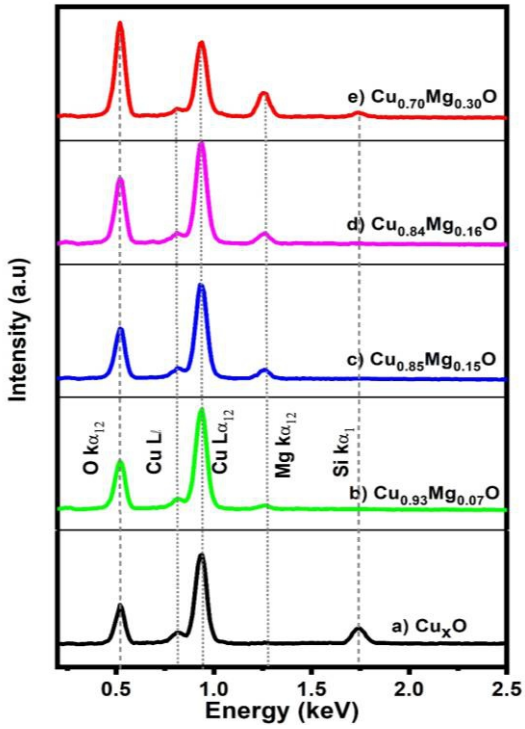

Figure 2: Energy dispersive X-ray spectra of Cu-O and Cu-Mg-O thin films deposited by reactive sputtering by applying a constant RF power (100 W) at the Cu target and varied RF power to Mg target: a) 0 W, b) 100 W, c) 150 W, d) 200 W, and e) 250 W.

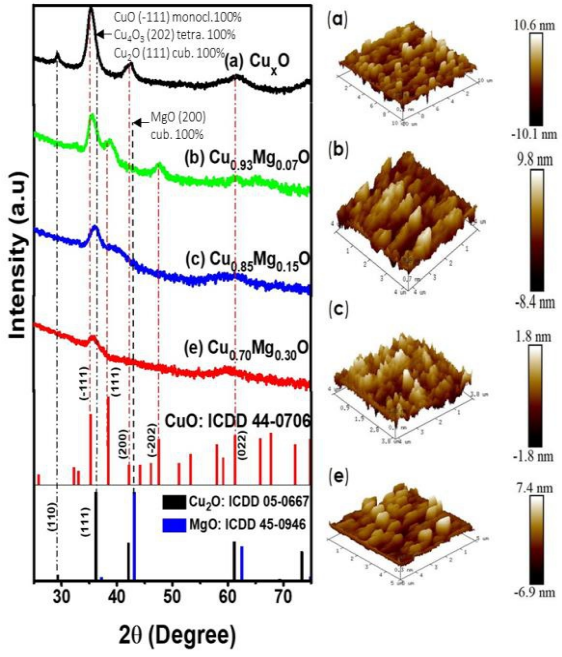

Figure 3: GIXRD patterns of (a) Cu_xO film and of (b, c and e) Cu-Mg-O films with different compositions. Side panel shows AFM images of the surface morphology of the corresponding films.

Figure 3 shows the GIXRD patterns of the films of Cu_xO (a) and of the different Cu-Mg-O films (b), (c), and (e). Here, the film (a) should be of composition Cu-O, because the RF power applied at the Mg target was zero. The pattern (a) shows peaks corresponding to (-111), (200), and (022) planes of CuO monoclinic structure (ICDD- 44-0076). The (110) peak of Cu_2O (ICDD- 05-667) seen at 2θ of 29.55° confirms the presence of this material in the film. Thus, CuO and Cu_2O coexist in the film. However, an exact assignment requires careful attention, when Cu, with its oxidation states Cu^+ and Cu^{++} available in the gas phase produced by the Ar-sputtering condenses into a solid phase in presence of oxygen available in the sputtering ambient. In the formation of Cu-O minerals, tenorite $Cu^{++}O$ (CuO), has a monoclinic structure (*a*, 4.653; *b*, 3.425; *c*, 5.129 Å; *β*, 99.467°) with four formula units per unit cell and a mass density of 6.55 g/cm^3. Cuprite, $(Cu^+)_2O = Cu_2O$ crystallizes into a cubic structure (*a*, 4.269 Å) with two formula units in the unit cell, with a mass density of 6.11 g/cm^3. Also present in copper mines (in Arizona and Michigan, USA) is parameloconite (03-0879), $(Cu^+)_2(Cu^{++})_2O_3 = Cu_4O_3$ with a tetragonal crystal structure (*a*, 5.83; *c*, 9.88 Å) with four formula units per unit cell, and a mass density 6 g/cm^3. The diffraction peaks corresponding to the maximum intensity from the crystalline planes seen in the XRD pattern overlaps at 2θ of nearly 36° for these three materials: CuO (-111) at 35.389°; Cu_4O_3 (202) at 35.891°, and Cu_2O (111) at 36.418°. In the absence of more detailed sample preparation and results, we designate the composition of film (a) as, Cu_xO.

The XRD patterns in (b), (c) and (e) are of the films grown by reactive RF co-sputtering (Ar +O_2) of Cu and Mg. The sputtered atoms from the Mg-target in the oxygen ambient can react to condense into MgO into the film or may substitute copper sites. We observe that in sample (b) produced with equal RF power (100 W) at the two targets, the sputter dynamics changes. The Cu_2O (110) peak disappears from the XRD pattern, implying that the sputtered atoms from the Cu-target have an abundance of oxygen to form CuO. The sputtering rate from Mg-target is typically 2/3 as from a Cu-target (Section 3.3), thus the overall film thickness drops to 280 nm. The mineral periclase, MgO, crystallizes into rock salt structure (*a*, 4.203 Å, file, 43-1022) with four formula units per unit cell and mass density, 3.61 g/cm^3. The close-by atomic numbers of the elements (O, 8; Mg, 12) leave the diffraction from the (111) planes with a very low intensity, at 2θ of 37.016°, but the diffraction peak from the (200) planes is intense (100%) at 43.005°, and so is also the diffraction peak arising from the (220) planes, at 62.446°. We do not observe these diffraction peaks in the patterns (b), (c) or in (e) produced with RF power 250 W at the Mg-target.

With an appreciable Mg-content in the film (e) of 30%, suggested from the EDS results, the absence of MgO diffraction peaks in the XRD pattern of the film suggests that Mg^{++} substitutes Cu^{++} sites in CuO. The absence of (110) diffraction peak of Cu_2O in (b) – (e) shows that Cu^+ sites are absent, and thus, Cu_4O_3 would also be absent. The ionic radii of Mg^{++} and Cu^{++} are the same, 0.072 nm (72 pm). [25] Hence, such substitution would not alter the monoclinic unit cell constants, and hence the XRD peaks would maintain their 2θ position. The Mg-substitution of the Cu-sites would however, lead to a decrease in the intensity of XRD peaks, because the atomic scattering factor (proportional to the electron cloud), which is decisive toward the diffraction peak intensity, is less at the Mg-site than at the Cu-site. Further, we observed a decrease in the thickness of the film with an increase in the sputtering power at the Mg-target while maintaining constant Ar (10 sccm)-O_2 (2 sccm) pressure at 3.5 mtorr in the chamber and the duration, 60 min. Film (b) is of 280 nm and (e), of 100 nm in thickness; the decrease arising from the reduced sputtering rate at the Mg-target (Section 3.3.). The enthalpy of formation[25] of MgO (– 602 kJ/mol) compared with that of CuO (– 157 kJ/mol) shows that Mg would readily replace Cu-sites in thin films and form Cu-Mg-O. The crystallite diameters in the films calculated using Scherrer equation for the diffraction peak at 2θ 35-36° are: (a), 103 Å; (b), 96 Å; (c), 90 Å; and (e), 88 Å. A similar trend in crystalline size was reported by Yirui Lv et al[26] in their investigation on Mg doped CuO for antibacterial activity. AFM images of the Cu-Mg-O thin films (a), (b), (c) and (e) are shown in the side panel of Figure 3. The average surface roughness was below 2 nm for all these films, which indicates that the film surface has desirable quality for electronic device applications.

3.2 Electrical conductivity.

Figure 4 shows the electrical conductivity (*σ*) of the Cu_xO film (a) and of the Cu-Mg-O films (b) to (e), evaluated from the photocurrent response measurements on these. Upon illumination, *σ* of the films increases due to the photo-generated carriers. A p-type *σ* of 10^{-5} to 10^{-4} Ω^{-1} cm^{-1} may be suitable for the film to work as an optical absorber in solar cells because in that case the thickness of the film required for a complete absorption of solar radiation can match the depletion region of the junction on the p-side.

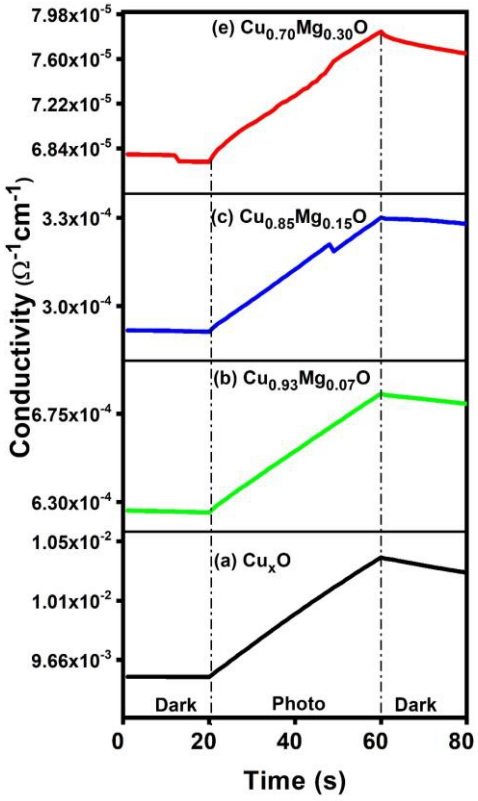

Figure 4: Electrical conductivity of – (a) Cu_xO thin film and of (b) – (e) Cu-Mg-O films, showing the increase in the value upon illumination (Photo) in all the films.

We find that σ of the Cu-Mg-O films decreases with the addition of Mg in the film: from 9.6 x 10^{-3} Ω^{-1} cm^{-1} for the film (a) - Cu_xO, to 6.7 x 10^{-5} Ω^{-1} cm^{-1} for the film (e) - $Cu_{0.7}Mg_{0.3}O$. To account for the reduction in σ, we may first recognize that the film (a) is nearly three times thicker than film (e) of 100 nm. The carrier transport takes place closer to surfaces in thinner films; hence, additional scattering loss and a reduction in the carrier drift mobility occurs in the film (e). A fall in the electrical conductivity of the films can also be due to the reduced polaron hopping conduction in doped CuO thin films.[27, 28] Mg^{2+} ions replacing the Cu^{2+} sites in the crystalline structure of CuO maintains the mobile holes and Cu vacancies, but appears to reduce the mobility of the charge carriers. Mg ions, irrespective of similar size as of Cu^{2+}, may alter the charge transport because the electronic cloud density at the site differs due to the difference in their atomic numbers (12 and 29). A decrease in the electrical conductivity in the Cu-Mg-O films with an increase in Mg content offers design options for solar cell development. However, to rule out the effect of thickness on σ, the thickness of the film (e) should be raised to 300 nm, which may require much longer duration of deposition, increased chamber pressure (> 3.5 mtorr) or of the RF power (> 250 W at Mg-target). Such conditions are not presently available to us.

3.3 Optical properties

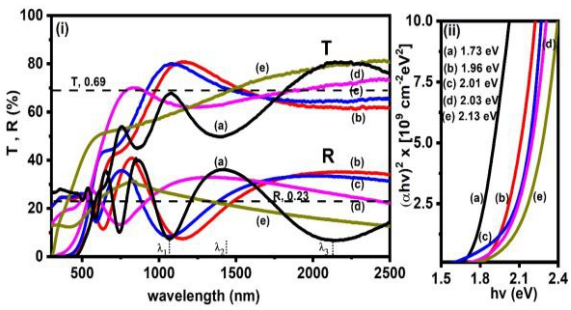

Figure 5: **i**) Optical transmittance (T) and reflectance (R) spectra of (a) CuxO and (b) – (e) of Cu-Mg-O films. At long wavelengths (1500 – 2500 nm) of the radiation, the average reflectance (R = 0.23) and the average transmittance (T = 0.69) add up to 0.92 (92 %), showing the near-specular nature of the film surface at this spectral region. The wavelength λ_3, λ_2, λ_1, marked for the adjacent crusts or troughs for the film (a) helps determine its thickness, 370 nm, and similarly for the other films. **ii**) Tauc plots, $(\alpha h\nu)^2$ versus $h\nu$ for the analysis of direct bandgap of the films.

Optical transmittance (T) and reflectance (R) spectra of the Cu_xO film (a) and of the Cu-Mg-O films (b) – (e) are presented in Figure 5 (**i**). At long wavelengths (1500 – 2500 nm) of the radiation, the average reflectance (R = 0.23) and the average transmittance (T = 0.69) add-up to 0.92 (92%), showing the near-specular nature of the film surface at this spectral region. This conclusion is in agreement with the AFM results in Figure 3, with surface roughness within ± 10 nm for the films, which is much less than the wavelength of the incident radiation. The wavelengths λ_3, λ_2, λ_1, marked for the adjacent crests or troughs for the film (a) help determine its thickness, and similarly for the other films: The specular reflectance R of 0.23 (23%), shown by the dotted line is representative for all the films. In electromagnetic theory, R is related to the refractive index (n) of the reflecting material in the spectral region, away from band-to-band absorption by:

$R = (n - 1)^2/(n + 1)^2$. From this, relation,

$n = (1 + R^{½})/(1 - R^{½})$, which assigns it a value of 2.84 for the films. The film thickness (d) is related to n and wavelengths of the adjacent trough and crest in the reflectance (or transmittance spectra) through $d = \lambda_2\lambda_1/4n\Delta\lambda$, where $\lambda_2 - \lambda_1 = \Delta\lambda$. This way, the film thicknesses for the films are: (a), 370 nm; b, 260 nm; c, 220 nm; d, 150 nm, and e, 75 nm, in general agreement with the values obtained from the step-measurement. Thus, as the RF power increased at the Mg-target to 250 W (power density, 5.5 W/inch^2, considering its 3-inch or 7.6 cm target diameter), the available Ar – ions are shared

at the Cu target (100 W fixed, power density, 2.2 W/inch^2) and at the Mg -target. The leads to a reduction in the film thickness at a fixed duration of sputtering (60 min = 3600 s) and the fixed chamber pressure (3.5 mtorr). The Ar-sputter rate is considerably lower for Mg (20 nm/s) than that of Cu (32 nm/s) for the same target-to-substrate distance (10
cm) as here, but at a much higher power, 250 W/inch^2, for an industrial-type sputtering system: For each Ar^+ ions of 600 eV energy striking a Cu-target, an estimated 2.4 Cu atoms are ejected, while on Mg-target, only 1.4 atoms are ejected (sputter yield estimates – fraction of atoms is accepted in this
expression). This difference among the behavior of sputtering targets in the same ambient provides a qualitative explanation for the reduction in thickness in the film (e).

The optical absorption coefficient (α) of the films was estimated from T and R data using the equation:[26]

$T = [(1 - R)^2 e^{-\alpha d}]/(1 - R^2 e^{-2\alpha d})$, where d is the film thickness.

Plots of $(\alpha h\nu)^2$ versus $h\nu$) of the films are shown in Figure 5 **ii**) for the analysis of direct bandgap of the films. With an increase in the Mg-content in the Cu-Mg-O films, there is an increase in the E_g of the films: (a) CuO, 1.73 eV; (b) $Cu_{0.93}Mgi_{0.07}O$, 1.96 eV; (c) $Cu_{0.85}Mg_{0.15}O$, 2.01 eV; (d) $Cu_{0.84}Mg_{0.16}O$, 2.03 eV; (e) $Cu_{0.70}Mg_{0.30}O$, 2.13 eV. The Cu-Mg-O films with such an interval of E_g may offer band alignment with various buffer layers in solar cells. However, one also would consider the variation in thickness and in the crystalline grain diameter among these films – the thickness of (a) nearly three times as in (e), before reaching more definite conclusions. The bandgap increases from a reduction in crystalline grain size, 96 Å in (b) and 88 Å in (e), compared with 103 Å in (a) due to the quantum confinement of excitons within it.

An overall outcome of the result presented above is that the reactive sputter deposition of Cu-Mg-O film allows for changing the Mg-content in the film by increasing or decreasing the RF power on the Mg-target during the deposition. This offers the possibility to vary the bandgap and the electrical conductivity along the thickness of the Cu-Mg-O film, without affecting the monoclinic unit cell dimension because of nearly the same size (72 pm) of Mg^{++} and Cu^{++}. We hope this possibility offers new design strategies in CdS/Cu-Mg-O solar cells. Here, other materials as well can substitute the CdS window, example ZnO:Co, reported in a 2020 work.[23] In Section 3.5 we shall find that such options can help reduce the band offsets and improve the Cu-Mg-O solar cells reported in Section 3.4.

3.4 Cu-Mg-O Solar cells

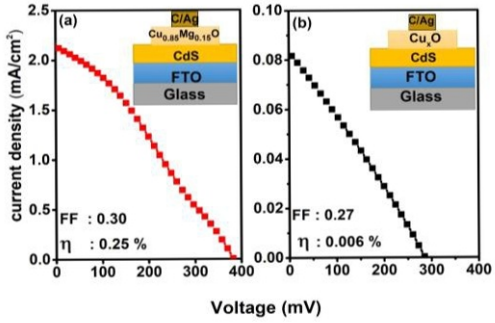

Figure 6: Current density (J) versus bias voltage (V) for the solar cell structures: (a) FTO/CdS(320 nm)/$Cu_{0.85}Mg_{0.15}O$ (360 nm)/C-Ag and (b) FTO/CdS (300 nm)/Cu_xO (340 nm)/C-Ag.

Figure 6 shows the current density (J) - voltage (V) characteristics of solar cells incorporating the films of $Cu_{0.85}Mg_{0.15}O$ and Cu_xO as absorbers. The corresponding cell structures are given as insets in Figure 6. The cell with $Cu_{0.85}Mg_{0.15}O$ shows better photovoltaic parameters, shown in Fig 5 (a): J_{sc} of 2.16 mA/cm^2; V_{oc} of 378 mV; and efficiency (η) of 0.25 % with a Fill Factor of 0.3, compared with the cell using the Cu_xO absorber Fig. 5 (b): J_{sc}, 0.08 mA/cm^2; V_{oc}, 284 mV; and η of 0.006. The solar cell parameters given in Table 1 were stable after more than three months of repeated measurements under a solar simulator. Thus, the preliminary results indicate that Cu-Mg-O films are worthy to be investigated further as a solar cell absorber material that consists of relatively higher abundant and less toxic elements. Optimization of the composition along the thickness of the absorber films and the use of appropriate contact and window layers offer opportunity for further work. A knowledge of the band alignment at the junction helps developing better solar cells of these materials.

Table 1. Parameters of Cu_xO and $Cu_{0.85}Mg_{0.15}O$ based solar cells

Solar cell structure	FF	V_{oc}	J_{sc}	η%	CBO
FTO/CdS/ Cu_xO/C	0.27	284 mV	0.08 mA/cm^2	.006	-0.90 eV
FTO/CdS/ $Cu_{0.85}Mg_{0.15}O$/CdS/C	0.30	378 mV	2.16 mA/cm^2	0.25	-0.75 eV

3.5 Band offset studies:

Band offsets at $Cu_{0.85}Mg_{0.15}O$/CdS interface were determined using depth profile XPS analysis. The XPS spectra of the $Cu_{0.85}Mg_{0.15}O$ solar cells given in Figure 7 show the interfaces between layers clearly identifiable. With the argon-etch up to 270 s, the cell shows only the peaks due to Cu 2p, Mg 1s and O 1s that belong to $Cu_{0.85}Mg_{0.15}O$ in its XPS spectra. However, after 300 s of etching, Cd 3d and S 2p peaks appear in the XPS, which indicates the $Cu_{0.85}Mg_{0.15}O$/CdS interface of the cell. Further etching of the cell resulted in a decrease in intensity of the XPS peaks corresponding to Cu, Mg and O, while the peaks due to Cd and S become dominant.

From the XPS data, we calculated the valence band offset (VBO) at the $Cu_{0.85}Mg_{0.15}O$/CdS interface using the equation [30]:

$$VBO = (E_{Cu\ 2p3/2\ (Cu0.85Mg0.15O)} - E_{VBM\ (Cu0.85Mg0.15O)}) - (E_{Cd\ 3d5/2(CdS)} - E_{VBM\ (CdS)}) - (E_{Cu\ 2p3/2\ (Cu0.85Mg0.15O/CdS\ )} - E_{Cd\ 3d5/2\ (\ Cu0.85Mg0.15O/CdS)}). \quad (1)$$

Here, $E_{Cu2p3/2(Cu0.85Mg0.15O)}$ and $E_{VBM\ (Cu0.85Mg0.15O)}$ are the binding energies of Cu $2p_{3/2}$ and VBM, respectively, measured for the $Cu_{0.85}Mg_{0.15}O$ film. $E_{Cd3d5/2(CdS)}$ and $E_{VBM(CdS)}$ are the binding energies of Cd $3d_{5/2}$ and VBM, respectively, obtained for the CdS thin film. $E_{Cu2p3/2\ (Cu0.85Mg0.15O/CdS)}$ and $E_{Cd\ 3d5/2\ (Cu0.85Mg0.15O/CdS)}$ are the corresponding binding energies of Cu $2p_{3/2}$ and Cd $3d_{5/2}$ at the $Cu_{0.85}Mg_{0.15}O$/CdS interface.

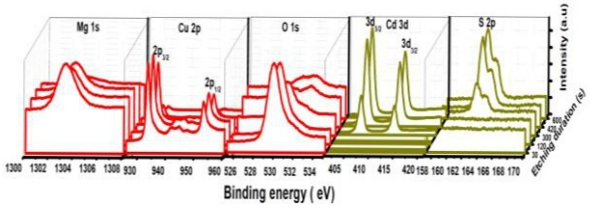

Figure 7: XPS depth profile taken for $Cu_{0.85}Mg_{0.15}O$ solar cell at progressive etching durations starting from 25 s to 800 s.

The valence band spectra of the thin films of $Cu_{0.85}Mg_{0.15}O$ and CdS are shown in Figure 8 (a) and (b). Extrapolating the linear part of the valence band leading edge to the binding energy axis gives the VBM of the film.[31] Figure 8 (c) illustrates the Cu 2p core level energy spectra from the $Cu_{0.85}Mg_{0.15}O$ film surface and $Cu_{0.85}Mg_{0.15}O$/CdS interface. Figure 8 (d) shows the Cd $3d_{5/2}$ core level spectra recorded for the CdS film surface and $Cu_{0.85}Mg_{0.15}O$/CdS interface. The VBO calculated using equation (1) for $Cu_{0.85}Mg_{0.15}O$/CdS interface was 1.18 ± 0.14 eV.

We calculated the conduction band offset for $Cu_{0.85}Mg_{0.15}O$/CdS interface using the following equation:

$$E_{CBO} = (E_{g(CdS\ )} - E_{g\ (Cu0.85Mg0.15O)}) - E_{VBO} \quad (2).$$

Here, $E_{g(CdS\ )}$ and $E_{g\ (Cu0.85Mg0.15O)}$ are the bandgaps of CdS and $Cu_{0.85}Mg_{0.15}O$ thin films, respectively. With $E_{g(CdS)}$ of 2.45 eV and $E_{g\ (Cu0.85Mg0.15O)}$ of 2.01 eV, the CBO is -0.74 ± 0.26 eV. The negative value of CBO indicates that the $Cu_{0.85}Mg_{0.15}O$/CdS is a Type-II heterojunction.[32] A small positive value of CBO (0 - 0.3 eV) is required for an ideal solar cell as it can prevent carrier recombination at the interface. For negative CBO values, a cliff will form at the Cu-Mg-O/CdS interface that reduces the activation energy for recombination and hence increases the rate of recombination at the interface. This may also be a reason for

the relatively lower values of photovoltaic parameters obtained in the $Cu_{0.85}Mg_{0.15}O$/CdS solar cell. In the same way, we have calculated the band offsets at the Cu_xO/CdS junction. Table 2 shows all the binding energy values used for VBO and CBO calculations. The VBO and CBO at the Cu_xO/CdS interfaces are 1.62 ± 0.14 eV and – 0.90 ± 0.14, respectively. The band energy diagrams made using these band offset values for the Cu-Mg-O/CdS and Cu_xO/CdS interfaces are as shown in Figure 8 (e) and 8 (f), respectively. Further investigation is required to replace CdS with a wide bandgap buffer layer like ZnO or ZnMgO, which can improve the band alignment with Cu-Mg-O and, thus, enhance the efficiency of the solar cell. A 2018 work[33] on Cu_2O/TiO_2 and CuO/TiO_2 heterojunction solar cell simulation reports an absorber band gap, light generated current density, and conversion efficiency of 2.17 eV, 11.8 mA/cm^2, and 9.45%, respectively, for the Cu_2O/TiO_2 (300 - 400 nm in thickness) solar cell and of 1.51 eV, 28.48 mA/cm^2, and 22.79%, respectively, for the CuO/TiO_2 solar cell. Thus, with a bandgap of 1.5 eV, close to that of CdTe and Perovskite structured absorber materials of the current high efficiency thin film solar cells, CuO holds bright prospects. Its modification in Cu-Mg-O films reported here opens up options.

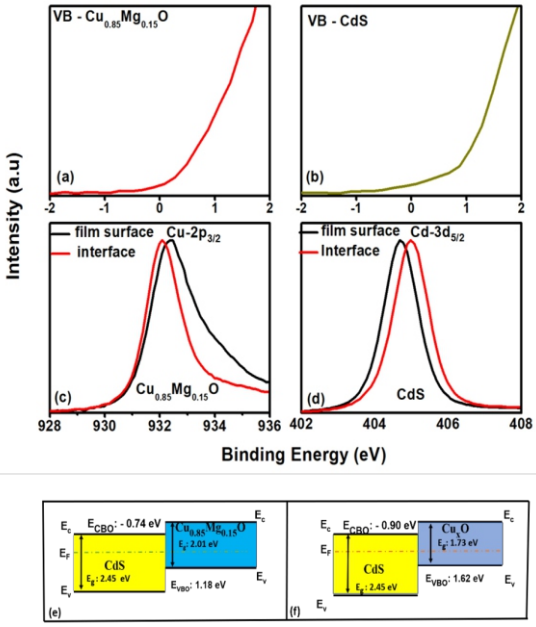

Figure 8: XPS spectra in valence band region for (a) $Cu_{0.85}Mg_{0.15}O$ and (b) CdS films; (c) XPS core level spectra in the region of binding energy corresponding to Cu taken from $Cu_{0.85}Mg_{0.15}O$ film and $Cu_{0.85}Mg_{0.15}O$/CdS interface; (d) XPS core level spectra in the region of binding energy corresponding to Cd taken from CdS film and $Cu_{0.85}Mg_{0.15}O$/CdS interface; (e) and (f) band diagrams of $Cu_{0.85}Mg_{0.15}O$/CdS and CuO/CdS heterojunctions.

Table 2. Core level binding energies and the location of VBM obtained from XPS for the different layers constituting the solar cell

Sample	Energy state	Binding energy (eV)
$Cu_{0.85}Mg_{0.15}O$	Cu $3p_{3/2}$	618.98
	VBM	0.97
Cu_xO	Cu $3p_{3/2}$	619.98
	VBM	1.46
CdS	Cd $3d_{5/2}$	458.33
	VBM	2.00
$Cu_{0.85}Mg_{0.15}O$/CdS	Cu $3p_{3/2}$	618.68
	Cd $3d_{5/2}$	458.18
Cu_xO/CdS	Cu $3p_{3/2}$	618.82
	Cd $3d_{5/2}$	458.25

4. Conclusion

Thin films of Cu-Mg-O with varying Mg composition were produced from commercially available Cu and Mg metal targets using a dual-magnetron reactive RF sputtering. The films show direct optical bandgaps in the range of 1.96 - 2.13 eV, as Mg content in the Cu-Mg-O film varies from 0.07 to 0.30, thereby maintaining the bandgap above that of the Cu_xO film (1.73 eV). The electrical conductivity decreases from 9×10^{-3} to 6.7×10^{-5} Ω^{-1} cm^{-1} as the Mg content in the film increases. A solar cell structure FTO/CdS/$Cu_{0.85}Mg_{0.15}O$/C-Ag showed a J_{sc}, 2.16 mA/cm^2 and V_{oc}, 378 mV. The conduction band offset (CBO) of – 0.74 ± 0.26 eV for $Cu_{0.85}Mg_{0.15}O$/CdS interface estimated from the XPS data indicates a Type-II heterojunction, which adversely affected the efficiency of the solar cell described in this work. We consider that the use of appropriate contact and window layers could produce a better band alignment with the $Cu_{0.85}Mg_{0.15}O$ layer. This, along with optimization of composition and thickness of the absorber films could improve the efficiency of these solar cells though future work.

5. Acknowledgment

We are grateful to María Luisa Ramón Garcia for the XRD measurements, to Jose Campos for EDS and electrical measurements, and to Oscar Gomez Daza for general laboratory support. We acknowledge Dr. Shaji Sadasivan, FIME-UANL for advising us on the XPS measurements. Financial support for the work came from CONACYT–SENER project CeMIESol 50 and DGAPA-PAPIIT UNAM projects IN116015 and IN109719. KCS acknowledges a postdoctoral fellowship awarded for this work by SENER-CONACYT-México.

References

1. L. De Los Santos Valladares, D. H. Salinas, A.B. Dominguez, D. A Najarro, S. Khondaker, T. Mitrelias, C. Barnes, J. Aguiar, and Y. Majima, Crystallization and electrical resistivity of Cu_2O and CuO obtained by thermal oxidation of Cu thin films on SiO_2/Si substrates, *Thin Solid Films*, **520**, 6368 (2012).

2. K. H. Yoon, W. J. Choi, and D. H. Kang, Photoelectrochemical properties of copper oxide thin films coated on an n-Si substrate, *Thin Solid Films*, **372**, 250 (2000).

3. S. S. Chang, H. J. Lee, and H. J. Park, Photoluminescence properties of spark-processed CuO, *Ceram. Int*., **31**, 411 (2005).

4. K. Han and M. Tao, Electrochemically deposited p–n homo- junction cuprous oxide solar cells, *Sol. Energy Mater. Sol. Cells*, **93**, 153 (2009).

5. S. Steinhauer, E. Brunet, T. Maier, G. Mutinati, A. Kock, O. Freudenberg, C. Gspan, W.Grogger, A. Neuhold,

and R. Resel, Gas sensing properties of novel CuO nanowire devices, *Sens. Actuators B. Chem.*, **187**, 50 (2013).

6. Y.Tokura, H. Takagi, and S. Uchida, A superconducting copper oxide compound with electrons as the charge carriers, *Nature*, **337**, 345 (1989).

7. G. Ren, D. Hu, E. W. Cheng, M. A. Vargas-Reus, P. Reip, and R. P. Allaker, Characterisation of copper oxide nanoparticles for antimicrobial applications, *Int. J. Antimicrob. Agents*, **33**, 587–590 (2009).

8. N. Kikuchi and K. Tonooka, Electrical and structural properties of Ni-doped Cu_2O films prepared by pulsed laser deposition, *Thin Solid Film*, **486**, 33 (2005).

9. K. C. Sanal, L .S. Vikas and M. K. Jayaraj, Room temperature deposited transparent p-channel CuO thin film transistors *Appl. Surf. Sci.*, **297**, 152 (2014).

10. M. Al-Kuhaili, Characterization of copper oxide thin films deposited by the thermal evaporation of cuprous oxide (Cu_2O), *Vacuum*, **82**, 623 (2008).

11. M. T. S. Nair, L. Guerrero, O. L. Arenas, and P. K. Nair, Chemically deposited copper oxide thin films: structural, optical and electrical characteristics*, Appl. Surf. Sci.*, **150**, 143 (1999).

12. Y. Gullen, F. Bayansal, B. Sahin, H. A. Cetinkara, and H. S. Guider, Fabrication and characterization of Mn-doped CuO thin films by the SILAR method, *Ceram. Int.*, **39**, 6475 (2013).

13. A. Brazdeikis, U. O. Karlsson, and A. S. Flodstrom, An atomic force microscopy study of thin copper oxide films grown by molecular beam epitaxy on MgO(100), *Thin Solid Film*, **281**, 57 (1996).

14. I. Y. Erdoğan and O. Güllü, Optical and structural properties of CuO nanofilm: its diode application, *J. Alloys Compd.*, **492**, 378 (2010).

15. K. C. Sanal and M. K. Jayaraj, Development of p-type amorphous $Cu_{1-x}B_xO_{2-d}$ thin films and fabrication of pn hetero junction, *Mater. Sci. Eng. B*, **185**, 109 (2014).

16. K. C. Sanal and M. K. Jayaraj, Room temperature deposited p-channel amorphous $Cu_{1-x}Cr_xO_{2-d}$ thin film transistors, *Appl. Surf. Sci.*, **315**, 274 (2014).

17. M. Nolan and S. D. Elliott, Tuning the Transparency of Cu_2O with Substitutional Cation Doping, *Chem. Mater.*, **20**, 5522 (2008).

18. J. Resende, C. Jiménez, N. D. Nguyen, and J. L. Deschanvres, Magnesium-doped cuprous oxide (Mg:Cu_2O) thin films as a transparent p-type semiconductor, *Phys. Status Solidi Appl. Mater. Sci.*, **213**, 2296 (2016).

19. R. Nagarajan, A. D. Draeseke, A. W. Sleight, and J. Tate, *p*-type conductivity in $CuCr_{1-x}Mg_xO_2$ films and powders, *J. Appl. Phys.*, **89**, 8022 (2001).

20. S. Masudy-Panah, G. K. Dalapati, K. Radhakrishnan, A. Kumar, H. R. Tan, E. N. Kumar, C. Vijila, C. C. Tan, and D. Z. Chi, p-CuO/n-Si heterojunction solar cells with high open circuit voltage and photocurrent through interfacial engineering, *Prog. Photovolt.*, **22**, 637 (2015).

21. S. Masudy-Panah, K- Radhakrishnan, H. R. Tan, R. Yi, T. I. Wong, and G. K. Dalapati, itanium doped cupric oxide for photovoltaic application, *Sol. Energy Mater. Sol. Cells*, **140**, 266 (2015).

22. A. Bhaumik, A. Haque, P. Karnati, M. F. N. Taufique, R. Patel, and K. Ghosh, Coopper oxide based nanostructures for improved solar cell efficiency, *Thin Solid Films*, **572**, 126 (2014).

23. A. Kaphle, E. Echeverria, D. N. McLlroy, and P. Hari, Enhancement in the performance of nanostructured CuO–ZnO solar cells by band alignmen, *RSC Adv.*, **10**, 7839 (2020).

24. M. T. S. Nair, P. K. Nair, R. A. Zingaro, and E. A. Meyers, Conversion of chemically deposited photosensitive CdS thin films to n-type by air annealing and ion exchange reaction, *J. Appl. Phys.*, **75**, 1557 (1994).

25. G. H. Aylward and T. J. V. Findlay, *S I chemical data*, 2nd ed., p. 44–72, Wiley, Milton, (1974).

26. Y. Lv, L. Li, P. Yin, and T. Lei, Synthesis and evaluation of the structural and antibacterial properties of doped copper oxide, *Dalt. Trans.*, **49**, 4699 (2020).

27. A. Yildiz, Horzum, N. Serin, and T. Serin, Hopping conduction in In-doped CuO thin films, *Appl. Surf. Sci.*, **318**, 105 (2014).

28. S. Horzum, A. Yildiz, N. Serin, and T. Serin, Carrier transport in In-doped CuO thin films, *Philos. Mag. Let.*, **93**, 3110 (2013).

29. J. I. Pankove, *Optical Processes in Semiconductors*, p. 36, 94., Dover, New York, (1975).

30. E. A. Kraut, R. W. Grant, J. R.Waldrop and S. P. Kowalczyk, Precise Determination of the Valence-Band Edge in X Ray Photoemission Spectra, *Phys. Rev. Lett.*, **44**, 1620 (1980).

31. M. Kumar, M. K. Rajpalke, B. Roul, T. N. Bhat, A. T. Kalghatgi, and S. B. Krupanidhi, Determination of MBE grown wurtzite GaN/Ge_3N_4/Ge heterojunctions band offset by X-ray photoelectron spectroscopy, *Phys. Status Solidi B*, **249**, 58 (2012).

32. A. M. Abdel Haleem and M. Ichimura, Experimental determination of band offsets at the SnS/CdS and SnS/InS xOy heterojunctions, *J. Appl. Phys.*, **107,** 34507 (2010).

33. P. Sawicka-Chudy, M. Sibiński, G. Wisz, E. Rybak-Wilusz, and M. Cholewa, Numerical analysis and optimization of Cu_2O/TiO_2, CuO/TiO_2, heterojunction solar cells using SCAPS, *J. Phys. Conf. Ser.*, **1033**, 1 (2018).